PERSPECTIVE

Check for updates

Porphyrinoids as a platform of stable radicals

Daiki Shimizu [ID] and Atsuhiro Osuka [ID]*

The non-innocent ligand nature of porphyrins was observed for compound I in enzymatic cycles of cytochrome P450. Such porphyrin radicals were first regarded as reactive intermediates in catabolism, but recent studies have revealed that porphyrinoids, including porphyrins, ring-contracted porphyrins, and ring-expanded porphyrins, display excellent radical-stabilizing abilities to the extent that radicals can be handled like usual closed-shell organic molecules. This review surveys four types of stable porphyrinoid radical and covers their synthetic methods and properties such as excellent redox properties, NIR absorption, and magnetic properties. The radical-stabilizing abilities of porphyrinoids stem from their unique macrocyclic conjugated systems with high electronic and structural flexibilities.

1. Introduction

Porphyrins and related macrocycles[1] play important roles in nature, as exemplified by the special pair of chlorophylls in the photosynthetic reaction center (RC), hemes, and cyano-cobalamine (vitamin B_{12}), to fulfill various biofunctions. Key features of these "pigments of life" are redox-active behaviors, coordination abilities, and light-harvesting properties. For example, the special pair of chlorophyll in the RC, upon photoexcitation, transfers an electron to an acceptor to form its radical cation, which triggers subsequent electron transfer events in photosynthesis known as the Z-scheme.[2a] Another example is cytochrome P450, which acts as a hydroxylation catalyst *via* the involvement of a radical cation intermediate (known as compound I; Fig. 1).[2b] Therefore, radicals and radical ions of porphyrins have been extensively investigated as models of intermediates in key biochemical processes. These radicals are usually short-lived and highly reactive. On the other hand, recent studies have

revealed that some porphyrinoid radicals and radical ions are extremely stable.

Here, we review the exceptionally effective radical-stabilizing abilities of porphyrinoids, including porphyrins, ring-contracted porphyrins, ring-expanded porphyrins, and core-modified porphyrins. In early studies, radicals stabilized by porphyrinoids had been found serendipitously, but in recent studies it has been demonstrated that the installation of a porphyrinoid at an appropriate conjugative position can be a general strategy for producing a stable radical. Importantly, in most cases radicals have been stabilized by porphyrinoids to such an extent that they are tolerant of air, moisture, and silica gel column chromatography, so that they can be handled like usual organic molecules. In special cases, radicals can undergo chemical transformations for their further modification.

It has been shown that porphyrinoids, in particular expanded porphyrins, are a suitable platform for generating various electronic states such as Hückel and Möbius (anti) aromatic species.[1f–i] This ability has been attributed to their structural and electronic flexibilities. The structural flexibilities of expanded porphyrins allow facile conformational changes upon a change in the number of π-electrons. A representative example is hexaphyrin(1.1.1.1.1.1), which can exist as a planar 26π Hückel aromatic species **1** and a twisted 28π Möbius aromatic species **2**, which are both stable compounds (Fig. 2). The electronic flexibilities of porphyrinoids are closely related to the facile amine–imine (pyrrole–pyrrolenine) interconversion of their pyrrole segments. For example, porphyrins consist of two amine-type and two imine-type pyrroles and can accommodate 16–20π electronic states *via* changes in the amine or imine forms of the pyrroles.[3] Because the amine-type pyrroles can act as electron donors and the imine-type pyrroles can act as electron acceptors, porphyrins are subject to both oxidation and reduction. The stabilities of the resulting non- or anti-aromatic electronic states should be correlated with the macrocyclic aromatic stabilization energy.[4] The total aromatic stabilization
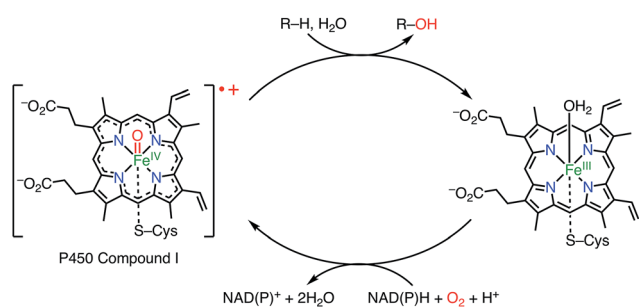

Fig. 1 Cytochrome P450 compound I.

Department of Chemistry, Graduate School of Science, Kyoto University, Kyoto 606-8502, Japan. E-mail: osuka@kuchem.kyoto-u.ac.jp
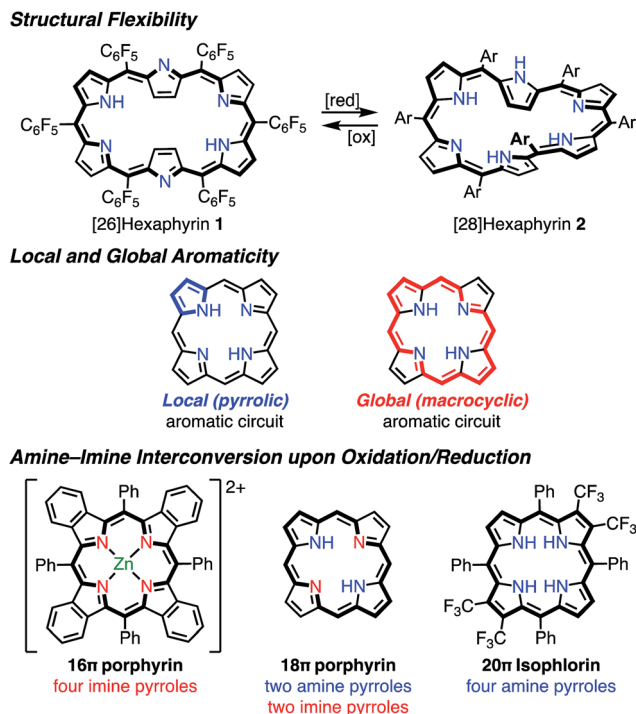
Structural Flexibility

[26]Hexaphyrin **1**   [28]Hexaphyrin **2**

Local and Global Aromaticity

Local (pyrrolic)   *Global (macrocyclic)*
aromatic circuit   aromatic circuit

Amine–Imine Interconversion upon Oxidation/Reduction

16π porphyrin   **18π porphyrin**   **20π Isophlorin**
four imine pyrroles   two amine pyrroles   four amine pyrroles
                           two imine pyrroles

Fig. 2 Important ideas for understanding the structural and electronic properties of porphyrins.

energies of porphyrinoids largely depend on the local aromaticity of the constituent pyrroles. Thus, the contribution of the macrocyclic aromatic stabilization energy is relatively small.[4b] Although the macrocyclic aromaticity is energetically low, aromatic porphyrinoids display an effective macrocyclic conjugated network as evidenced by strong diatropic ring currents, which are predominantly due to the global conjugation circuit. A theoretical interpretation of this specific balance between aromaticity and conjugation has been attempted.[4a] It is considered that these unique electronic and structural flexibilities generally play important roles in stabilizing radicals as well as aromatic and anti-aromatic species.

Although there are many studies of porphyrinoids that are covalently linked to or coordinated with stable localized radicals (*e.g.* nitroxides and nitronyl nitroxides),[5] this review will focus on organic radicals stabilized by spin delocalization over the π-electron systems of porphyrinoids.

2. Classification of porphyrinoid-based radicals

Porphyrinoid-based radicals can be classified into four types according to the origin of the radical, as shown in Fig. 3: (i) one-electron-oxidized/reduced radical ions (Chapter 3), (ii) substituent-centered neutral radicals (Chapter 4), (iii) non-innocent macrocyclic radicals of metal complexes (Chapter 5), and (iv) Kekulé/non-Kekulé-type diradicals (Chapter 6). Regardless of this classification, stable organic radicals are required to satisfy the following criteria: (1) effective
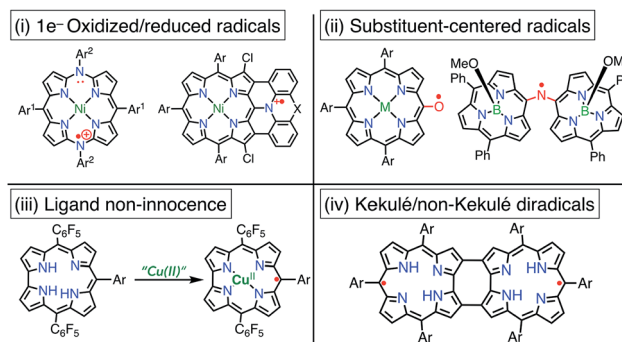

Fig. 3 Four types of porphyrinoid-based stable radicals.

delocalization of spin density for thermodynamic stabilization, (2) appropriate steric protection (kinetic stabilization) to avoid dimerization and undesired reactions, and (3) moderate redox potentials to prevent the facile reduction and oxidation of the radical itself. Therefore, most stable radicals are neutral species.

2.1. Methodologies for characterization of porphyrinoid radicals

Because porphyrinoid radicals have unique open-shell electronic structures, they should be characterized very carefully. For example, delocalized radicals are NMR-silent owing to fast electronic relaxations. Because NMR spectroscopy is not effective for radicals, the structural determination of radicals largely relies on X-ray diffraction analysis. When X-ray analysis is impossible, NMR characterizations of 1e⁻ oxidized or reduced compounds are also useful. EPR spectra with hyperfine couplings sometimes provide structural information, but porphyrinoid radicals frequently display isotropic signals around $g = 2$ without hyperfine structures. On the other hand, anisotropic EPR signals indicate the contribution of spin–orbit interactions with coordinated metals. Quantitative insights into spin states can be obtained by using VT-EPR, SQUID, and NMR studies. In the case of metalloporphyrinoids, the determination of the valence of the central metal is also important and is often provided by Mössbauer and X-ray photoelectron spectroscopies. The nature of the spin distribution can be estimated from hyperfine coupling constants in EPR spectra and *via* theoretical calculations.

3. One-electron-oxidized/reduced radical ions

Metalloporphyrins are easily oxidized or reduced to generate the corresponding radical cations or radical anions, which often occur not on the central metal but on the porphyrin macrocycle.[6] These transformations can be accomplished by chemical reactions or electrochemical methods, but the radical ions thus generated are mostly reactive and thus unstable.[7] However, in recent years, very stable porphyrinoid radical ions have been found. In this section, we discuss recent examples of stable radical ions of porphyrinoids.

3.1. Stable radical cations of porphyrinoids

Diazaporphyrin is a macrocycle in which two methine-carbon of porphyrin are replaced by nitrogen atoms. Matano *et al.* reported multi-redox processes of the 20π anti-aromatic 5,15-diazaporphyrins **3M** (M = Ni, Zn, Cu).[8] Owing to their electron-rich nature, **3M** exhibited multiple stable oxidation states. For example, two-electron oxidation of **3M** with AgPF$_6$ afforded 16π-electron dications **3M(PF$_6$)$_2$**, and subsequent reduction with NaBH$_4$ or CoCp$_2$ gave 19π-electron monocations **3M(PF$_6$)** as stable compounds (Fig. 4). The free-base derivative **3H$_2$(PF$_6$)** was also prepared *via* demetalation of the corresponding Mg(II) complex **3Mg** followed by chemical $1e^-$ oxidation. These radical cations were fairly stable under ambient conditions and were purified by silica gel column chromatography. The redox potentials of **3Ni(PF$_6$)** were determined by cyclic voltammetry to be $E_{ox1} = 0.29$ V $(20\pi/19\pi)$ and $E_{red1} = -0.37$ V $(19\pi/18\pi)$ *vs.* Ag/Ag$^+$ in CH$_2$Cl$_2$. Importantly, the mixing of **3Ni** and **3Ni(PF$_6$)$_2$** also afforded the radical cation **3Ni(PF$_6$)** as evidenced by the EPR spectrum, which exhibited hyperfine coupling with the two *meso*-nitrogen atoms and four β-protons. The absorption

spectrum of **3Ni(PF$_6$)** in toluene exhibited a characteristic band in the NIR region around 880 nm. **3Cu(PF$_6$)**, **3Zn(PF$_6$)**, and **3H$_2$(PF$_6$)** also displayed electrochemical and optical properties that were quite similar to those of **3Ni(PF$_6$)**. In the case of **3Cu(PF$_6$)**, a magnetic interaction between the paramagnetic Cu(II) center and the π-radical is possible. In fact, neither EPR nor NMR signals were observed, which was presumably due to large zero-field splitting and the contribution of the triplet state, respectively. However, the assignment of the ground state is under discussion. Intriguingly, **3Mg** was found to catalyze the dimerization of a phenyl Grignard reagent in the presence of air. NMR and EPR experiments suggested a mechanism involving a $20\pi/19\pi$ redox cycle of **3Mg**, as shown in Fig. 4. Shinokubo *et al.* also reported the diazaporphyrin **4** without substituents on the *meso*-nitrogen atoms.[9] In this case, a 19π species of the radical cation was not observed from the oxidation of the 20π species or the reduction of the 18π species **5**, which was presumably due to facile disproportionation of the cationic intermediate.

Osuka *et al.* synthesized the diphenylamine-fused porphyrins **6** and **7** (Fig. 5).[10] The lone-pair electrons of the embedded nitrogen atom were well conjugated with the extended porphyrin conjugated network, which caused a decrease in oxidation potentials. Chemical $1e^-$ oxidation gave the corresponding radical cations, both as unstable species. One of the degradation products was a β-chlorinated species, which indicated high spin density and reactivity at the β-position next to the fused moiety. To suppress this degradation pathway, **6** and **7** were chlorinated to give **8** and **9**. Chemical oxidation of **8** and **9** gave **8(SbCl$_6$)** and **9(SbCl$_6$)**, respectively, which were found to be extremely stable towards air, water, and silica gel column chromatography. As a result of this success, the diarylamine-fused porphyrin dimers **10** and **11** were prepared and their oxidation to the corresponding diradicals was attempted.[11] Upon oxidation with magic blue, however, **10** and **11** were

Fig. 4 Redox scheme of diazaporphyrins. (a) 2 equiv. AgPF$_6$, CH$_2$Cl$_2$, rt, 2 min, 85% for **3Ni(PF$_6$)$_2$**, 82% for **3Zn(PF$_6$)$_2$**, 75% for **3Cu(PF$_6$)$_2$**; (b) excess NaBH$_4$, THF, rt, 8 h, 77% for **3Ni(PF$_6$)$_2$**; (c) 1 equiv. NaBH$_4$ or CoCp$_2$, MeOH, 2 min, 80% for **3Ni(PF$_6$)**, 85% for **3Zn(PF$_6$)**, 75% for **3Cu(PF$_6$)**; (d) *N,N′*-bis(trimethylsilyl)-1,4-dihydropyrazine, THF, rt, 48 h, then MeOH, 78%; (e) aerobic oxidation; (f) 61 equiv. PhMgBr, toluene/THF, rt, 10 min, not isolated; (g) trifluoroacetic acid, 70 °C, 7 h, 38% from **3Zn(PF$_6$)**; (h) 1 equiv. AgPF$_6$, CH$_2$Cl$_2$, rt, 2 min, 30%. Ar^1 = Mesityl, Ar^2 = 4-methoxyphenyl.
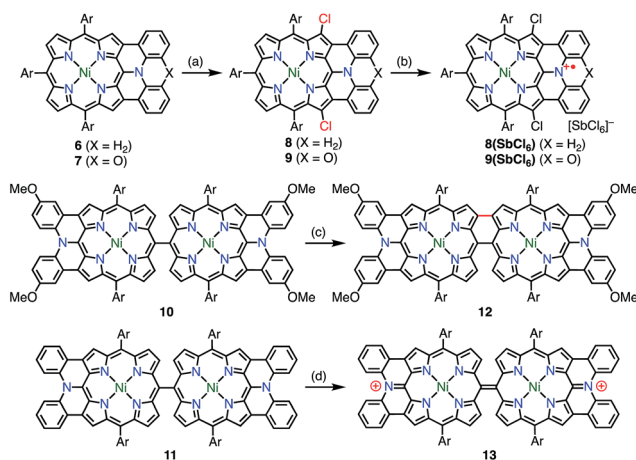

Fig. 5 Diarylamine-fused porphyrins. (a) 2.2 equiv. Palau'chlor, CHCl$_3$, 0 °C to rt, 87% for **8**, 77% for **9**; (b) 1.1 equiv. magic blue, CH$_2$Cl$_2$, rt, 10 min, 79%; (c) 6.0 equiv. magic blue, CH$_2$Cl$_2$, rt, 15 min, then H$_2$-NNH$_2$·H$_2$O, 91%; (d) 2.2 equiv. magic blue, CH$_2$Cl$_2$, 10 min, 72%. Ar = 3,5-di-*tert*-butylphenyl.

transformed into the partially fused dimer **12** and the closed-shell quinonoidal species **13**, respectively, instead of open-shell diradicals.

3.2. Stabilizing radical anions is a challenge

Although the properties of $1e^-$-reduced porphyrin radical anions have been investigated,[12] the isolation of stable radical anions of porphyrinoids has remained challenging. The reason is simply because porphyrinoids are usually electron-rich, and their radical anions are even more easily oxidized under aerobic conditions. Thus, the isolation of porphyrin radical anions has been difficult so far.

Whereas the SOMO orbital of radical cations reflects the characteristics of the HOMO of their neutral precursors, the SOMO orbital of radical anions represents the characteristics of the LUMO of their precursors. Therefore, the radical anions of porphyrinoids should have different electronic states from those of the radical cations, and it is also desired to investigate such radical anion species. Because most aromatic porphyrinoids have a $[4n + 2]\pi$-system, $[4n + 1]\pi$-radicals are easily accessible via the one-electron oxidation of neutral aromatic porphyrinoids, but $[4n + 3]\pi$-radicals are relatively difficult to generate. To the best of our knowledge, only two strategies for generating $[4n + 3]\pi$-radicals have been reported: (1) oxidative generation from stable $[4n]\pi$-species[8,13,14] and (2) the incorporation of a positively charged center into the electron-deficient chromophore to balance the charge.[15] Fig. 6 summarizes the important orbitals and optical transitions of a neutral molecule, a radical cation, and a radical anion of porphyrin. Both radical anions and cations display similar P_1 and P_2 absorption bands. Although the origins of the P_2 bands are similar for radical anions and radical cations, those of the P_1 bands are different. Here, we use the terms P_1 and P_2 bands to indicate the lowest-energy transition (P_1) and the following Q-like (P_2) band.[16,17]

4. Substituent-centered radicals

4.1. Heme catabolism and *meso*-oxy radicals

Heme is an iron complex of porphyrin that plays crucial roles in catalysis in heme proteins. However, once heme is released from the protein, it causes toxicity by generating reactive oxygen species. Therefore, the catabolism of heme is critically important in maintaining homeostasis. Because the first step of the catabolic process is known to be oxidation by heme oxygenase to give *meso*-oxyheme **15**,[18] its derivatives have attracted great interest (Fig. 7). The structure of **15** in heme oxygenase was determined to be **15A**, but the reactivity that was observed toward molecular oxygen implied the contribution of the π-radical **15B**.[19] Although Bonnett et al. reported 1% paramagnetism for the free base β-octaethyl-*meso*-hydroxyporphyrin **18H₂** in 1970,[20] it was a long time until the first structural characterization of the paramagnetic species, i.e., the *meso*-oxy radical (oxophlorin radical), in 1992.[21] Fuhrhop et al. investigated the reactivity of Zn(II) and Ni(II) complexes of the *meso*-oxy radical **19M** (M = Ni, Zn) generated in situ and found rapid and irreversible dimerization at the 15-position.[22]

Balch et al. later investigated a series of β-octaethylporphyrin (OEP) *meso*-oxy radicals.[23] They found that the oxidation of Zn(II) and Ni(II) *meso*-hydroxy OEP **18M** in the presence of pyridine gave the *meso*-oxy radicals **21Zn** and **21Ni** as stable compounds (Fig. 8).[21,24] X-ray diffraction analysis confirmed the axial coordination of the pyridine on the central metal. The coordinated pyridine was demonstrated to effectively stabilize the radical, because the removal of the pyridine led to the instantaneous dimerization of the radical. The radical **21Zn** had a short C_{meso}–O bond (1.268 Å) in comparison to that of **18Zn** (1.392 Å), which is a common feature of *meso*-oxy radicals. In **21Ni**, the
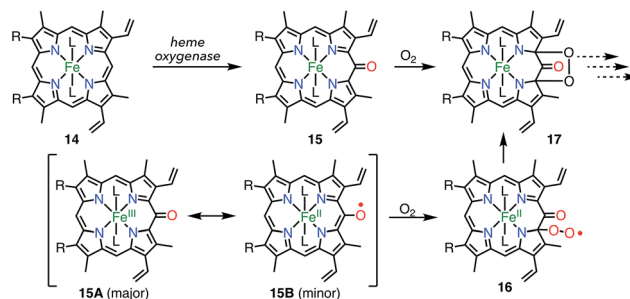

Fig. 7 Heme catabolism.

Fig. 6 Difference between radical cation and anion.

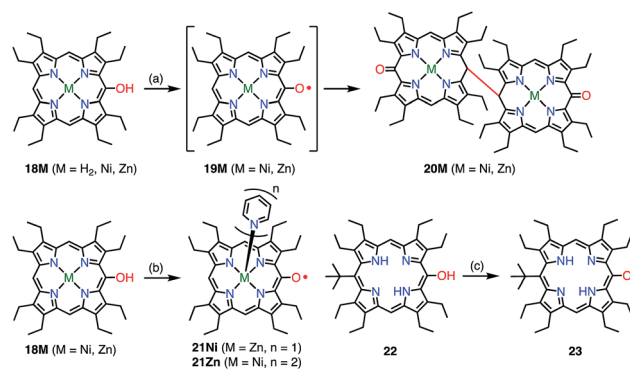**Fig. 8** Stable OEP *meso*-oxy radicals. (a) Electrochemical oxidation in CH₂Cl₂; (b) I₂, pyridine, rt, 15 min, 48% for **21Ni**; air, pyridine for **21Zn**; (c) air, daylight, CH₂Cl₂, 90%.

octahedrally coordinated Ni(II) atom had a high-spin ($S = 1$) state as evidenced by an increase in the Ni–N distance, which arose from population of the $d_{x_2-y_2}$ orbital. However, the EPR spectrum of **21Ni** in pyridine displayed a sharp signal at $g = 2.006$, and its magnetic moment was determined to be 2.5(2) μ_B, which indicated the $S = 1/2$ character of the ground state. These results were interpreted in terms of an antiferromagnetic interaction between the porphyrin π-radical and the high-spin Ni(II) center.

Smith *et al.* synthesized the free-base *meso*-oxy radical **23** bearing a *tert*-butyl group at the 15-position. Steric protection at the 15-position, where the highest spin density was expected, led to enhanced stability.[25] In fact, **23** displayed improved stability but underwent 30% degradation after two weeks in solution. By employing this strategy, the authors demonstrated an elegant way to construct *meso–meso*-linked oxophlorin oligomers by controlling radical–radical coupling.[26]

Osuka *et al.* attempted the synthesis of 15,30-bis(*meso*-free) [26]hexaphyrin(1.1.1.1.1.1) **24**.[13] The authors obtained **24** together with the *meso*-oxy radical **25** *via* the aerobic oxidation of **24** (Fig. 9). X-ray diffraction analysis of **25** revealed a planar structure with a short C_{meso}–O bond length of 1.281 Å, which indicated a highly delocalized spin distribution. As is typical for radical porphyrinoids, **25** displayed quite reversible oxidation and reduction waves with a small redox gap of 0.48 V. Furthermore, Osuka *et al.* found that the oxidation of **24** upon metalation with Ni(II) followed by demetalation gave the bis (*meso*-oxy) diradical **26**.[27] **26** was shown to be a stable non-Kekulé diradical, because SQUID magnetometry confirmed the singlet nature of its ground state with $J/k_B = -645$ K, and CASSCF(2,2) calculations showed an open-shell singlet diradical ground state with a diradical index of 0.62. Reflecting the singlet nature of the ground state, the ^{1}H NMR spectrum of **26** displayed signals due to β-protons at 8.0 and 9.6 ppm, as well as a signal due to the inner NH group at 4.5 ppm at -80 °C in CD$_2$Cl$_2$, which indicated a diatropic ring current in the 26π aromatic system. These signals became broader upon an increase in temperature owing to the population of the triplet diradical state. The aromaticity of **26** was further confirmed by theoretical calculations: an NICS(0) of -8.2 ppm and a net clockwise (diamagnetic) flow of current density in anisotropy of

current-induced density (ACID) calculations. To the best of our knowledge, this is the first observation of ground-state open-shell aromaticity.[28]

The observed high stabilities of **25** and **26** were considered to arise from effective spin delocalization over the large π-system of the hexaphyrin network. In 2015, however, the subporphyrin *meso*-oxy radical **28** was found to be very stable (Fig. 10).[29] *meso*-Hydroxysubporphyrin **27** was readily oxidized to **28** in the open air in solution, and a trace amount of **28** made the ^{1}H NMR spectrum of **27** completely silent, which was presumably due to rapid hydrogen exchange. The oxidation of **27** with PbO$_2$ gave the radical **28** in quantitative yields. An EPR study of **28** revealed hyperfine coupling with the protons of the *meso*-phenyl groups, as well as the subporphyrin core, which confirmed effective spin delocalization over the whole molecule except for the axial phenyl group. It is noteworthy that even a relatively small porphyrinoid such as 14π aromatic subporphyrin efficiently stabilizes the *meso*-oxy radical.

With the encouragement of these results, the 10,15,20-triarylporphyrin *meso*-oxy radicals **30M** (M = H$_2$, Ni, Zn) were synthesized by Osuka *et al.* (Fig. 11).[30,31] In comparison with the OEP-based radicals, the stabilities of the **30M** radicals were dramatically increased. Namely, the **30M** radicals were stable in solution under ambient conditions and were purified by silica
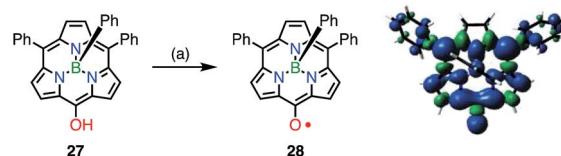

Fig. 10 Synthesis of the subporphyrin *meso*-oxy radical **28** and plot of spin density distribution of **28** (isovalue = 0.001). (a) 800 equiv. PbO$_2$, CH$_2$Cl$_2$, rt, quant.

Fig. 11 10,15,20-Triarylporphyrin *meso*-oxy radicals. (a) 800 equiv. PbO$_2$, CH$_2$Cl$_2$, rt, 5 min, 86% for **30H$_2$**, 91% for **30Ni**, 89% for **31**; (b) aerobic oxidation for **33**, 7 equiv. DDQ, CH$_2$Cl$_2$, rt, 30 min, 26% for **34**. Ar = 3,5-di-*tert*-butylphenyl. Hydrogen atoms and *tert*-butyl groups in the crystal structure of **31** were omitted for clarity.
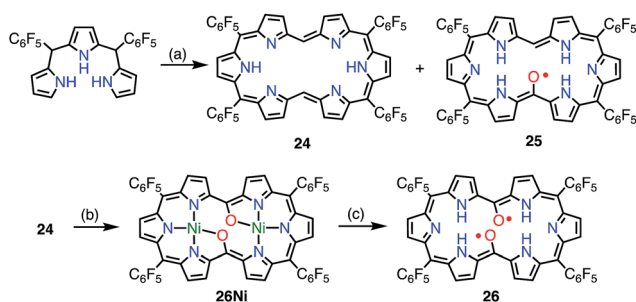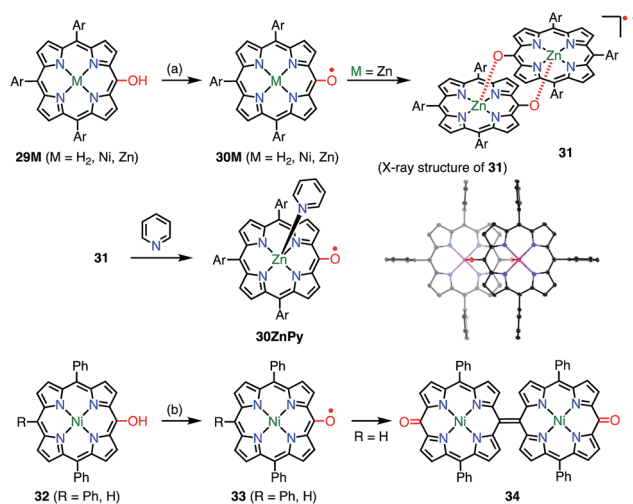

Fig. 9 Hexaphyrin mono- and bis(*meso*-oxy) radicals. (a) 22 equiv. HC(OMe)$_3$, 17 equiv. MeSO$_3$H, MS3A, CH$_2$Cl$_2$, 0 °C, 7 h in the dark, 17% for **24** and 15% for **25**; (b) *ca.* 10 equiv. Ni(acac)$_2$·nH$_2$O, CH$_2$Cl$_2$/MeOH, rt, 1 h, 24%; (c) *ca.* 900 equiv. MeSO$_3$H, CH$_2$Cl$_2$, rt, 30 min, 83%.

gel column chromatography. The Zn complex **30Zn** was found to form the complementarily coordinated dimer **31** both in solution and in the solid state. The dimer **31** underwent quantitative dissociation into the monomer **30ZnPy** on the addition of pyridine. The dimer exhibited a characteristic broad absorption band in the region of 1000–2000 nm, which was assigned to a symmetry-breaking charge transfer band. Although the optical and electrochemical properties were similar to those of the monomers regardless of the central metal, the magnetic properties of the solid states were strongly dependent on the metal. Namely, planar **30H₂** and **30Zn** formed efficiently overlapping π-dimers, which resulted in strong intermolecular antiferromagnetic interactions with $J/k_B = -790$ K (**30H₂**) and -720 K (**30Zn**). On the other hand, **30Ni** has a saddle-like structure and forms an offset π-dimer with $J/k_B = -110$ K. A strong intermolecular magnetic interaction *via* π–π stacking has also been revealed for porphyrin radical cations.[32] Coordination with pyridine interrupted such π-stacking and thus allowed **30ZnPy** to display an *M–T* curve that was typical of monoradical species. Arnold *et al.* also independently reported the facile aerobic oxidation of *meso*-hydroxyporphyrin **32** to furnish the radical **33**.[33] They showed that the lack of a 15-aryl group allowed the oxidative formation of the 15,15′-linked dimer **34**.

4.2. Carbon-centered radicals

In addition to diphenylborane-[34] and diphenylamine-fused porphyrins,[35] the synthesis of the diphenylmethane-fused porphyrin **35** was attempted *via* an intramolecular C–H arylation reaction of **36**.[36] Surprisingly, the isolated product was not **35** but the neutral radical **37Ni** *via* the loss of a hydrogen atom on the fused carbon atom (Fig. 12). The radical **37Ni** was very stable under ambient conditions and did not react with hydrogen donors such as *n*Bu₃SnH and ascorbic acid. Taking advantage of the robust stability of **37Ni**, its denickelation with sulfuric acid was accomplished to afford the free-base derivative **37H₂** in a yield of 51%. The high stabilities of **37Ni** and **37H₂** arise from effective spin delocalization over the whole molecule and the structural rigidification.[37] In a single crystal, both **37Ni** and **37H₂** form antiparallel π-stacked dimers with π–π distances of 3.51 and 3.56 Å for **37Ni** and 3.56 and 3.61 Å for **37H₂** together with an offset of 3.4–3.5 Å. The intermolecular exchange interaction in the solid state was determined to be $J/k_B = -391$ K (**37Ni**) and -279 K (**37H₂**), which reflected the slightly different π–π distances.

Because the externally fused moiety of **37** can be regarded as a helicene-like structure, an extended series of **37** derivatives has been synthesized to obtain stable neutral helically chiral radicals.[38] The bis(2-methylphenyl)methyl-, bis(2-methoxyphenyl)methyl-, and dinaphthylmethyl-fused porphyrins **39R** (**R** = Me or OMe) and **41** were synthesized *via* Pd-catalyzed intramolecular fusion reactions (**39R**) and an oxidative fusion reaction (**41**). **39R** and **41** are rare examples of stable radicals in which the spin is delocalized over a chiral π-system. Unfortunately, **39R** and **39R′** were obtained as a mixture of regioisomers owing to an unexpected rearrangement (**39Me**/**39Me′** = 32/68 and **39OMe**/**39OMe′** = 22/78), which was
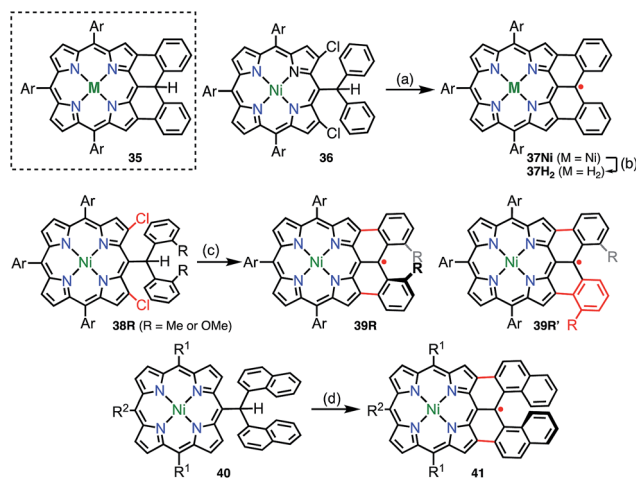

Fig. 12 Diarylmethyl-fused porphyrins. (a) 20 mol% Pd(OAc)₂, 40 mol% PCy₃·HBF₄, 5 equiv. K₂CO₃, toluene, reflux, overnight, 72%; (b) H₂SO₄/CF₃CO₂H, 0 °C to rt, 45 min, 51%; (c) 20 mol% Pd(OAc)₂, 40 mol% PCy₃·HBF₄, 5 equiv. K₂CO₃, toluene, reflux, overnight, 48% for **39Me/39Me′**, 79% for **39OMe/39OMe′**; (d) 10 equiv. DDQ, 10 equiv. Sc(OTf)₃, toluene, 110 °C, 1 h, 19%. Ar = 3,5-di-*tert*-butylphenyl, R¹ = mesityl, R² = 4-methylphenyl.

determined by analyzing 1e⁻-oxidized closed-shell cations [**39R**]⁺. The radical **41** was synthesized from **40** and was optically resolved using chiral HPLC. The circular dichroism spectra of the separated enantiomers exhibited weak but distinct mirror images up to 1400 nm. Because the lowest-energy band was assigned to the HOMO(β)–SOMO(β) transition, the circular dichroism observed in the NIR region indicated the spreading of the corresponding orbitals over the helical skeleton. In contrast to **37**, the radical **41** did not form a π-stacked dimer in the solid state, and the intermolecular magnetic interaction was found to be slight (Weiss temperature of −2.7 K), owing to unfavorable steric interactions at the ends of the helices.

4.3. *meso*-Aminyl radicals

In contrast to oxygen- and carbon-centered radicals, aminyl radicals are unstable, and adjacent heteroatoms are usually required for their stabilization. Heteroatoms next to the aminyl center stabilize aminyl radicals *via* effective spin sharing as seen in the cases of hydrazinyl, oxyaminyl, and thioaminyl radicals.[39] However, stable aminyl radicals without such adjacent heteroatoms are very rare, and the investigation of stable aminyl radicals without such resonance stabilization is a challenging issue. Osuka *et al.* attempted the oxidation of the *meso*-aminosubporphyrin **42R** with PbO₂ in the expectation that it might give the aminyl radical **43R**, but the reaction gave the azosubporphyrin **44R**, presumably *via* **43R** (Fig. 13).[40] Thus, *meso*-(2,4,6-trichlorophenyl)subporphyrin **45** was prepared and oxidized to provide the subporphyrin *meso*-aminyl radical **46R** in a high yield. Importantly, this radical was found to be fairly stable in spite of its neutral character without resonance stabilization.[41] The bis(subporphyrinyl)aminyl radical **47** was also synthesized and found to be even more stable. Both the hyperfine coupling constants of the pyrrolic nitrogen atoms (N²
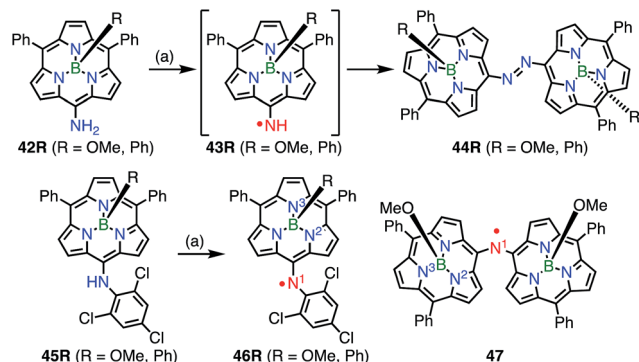
Fig. 13 Subporphyrin *meso*-aminyl radicals. (a) 200 equiv. PbO$_2$, CH$_2$Cl$_2$, rt, 5–10 min, 83% for **44OMe**, 95% for **44Ph**, 88% for **46OMe**, 87% for **46Ph**.

and N^3 in Fig. 13) and DFT calculations indicated a higher spin density on the nitrogen atom in comparison with that in the corresponding oxygen-centered radicals, which was presumably because the C=N bond energy is less than that of the C=O bond. Whereas both radicals (**46Ph** and **46OMe**) were quite stable, the spin delocalization over the subporphyrin core was more effective in **46Ph** than in **46OMe**, which may reflect the more electron-rich nature of **46Ph**.

5. Non-innocent macrocyclic radicals

In the previous section, we discussed ligand-centered redox processes of M(II) metalloporphyrinoids that led to the formation of stable radicals owing to the non-innocent ligand[42] character of porphyrinoids. In this section, we focus on other cases in which the redox-active character of porphyrinoid macrocycles enables the formation of stable radicals. Porphyrinoids can accommodate various metals. When the valence of the metal is mismatched with the cavities of the porphyrinoid and causes the complex to have a net charge, the resulting complexes sometimes tend to balance the charge by releasing or acquiring an electron (Fig. 14). These processes are facilitated by the fairly flexible π-networks of porphyrinoids.

5.1. Facile non-innocent behavior of porphyrinoids

Chandrashekar *et al.* reported that the metalation with Ni(II) of oxasmaragdyrin **48**, which is an expanded porphyrin bearing three pyrrolic protons, afforded a neutral π-radical *via* spontaneous oxidation of the macrocycle (Fig. 15).[43] The Ni(II) complex **49** displayed a sharp EPR signal at *g* = 2.0031 with a linewidth of 11 G, which can be assigned to organic π-radical species. It should be noted that **49** also exhibited a slightly broader but distinct ^{1}H NMR spectrum at 25 °C.

Osuka *et al.* reported that the metalation of [28]hexaphyrin with Pd(II) gave the bis-Pd(II) complex **50** together with the Möbius aromatic mono-Pd(II) complex **51** as a minor product (Fig. 16).[14] In **50**, [28]hexaphyrin acted as an inner 4NH ligand, but the bridging Cl$^-$ ion caused a valence mismatch. As a consequence, the hexaphyrin ligand released one electron to balance the charge to provide the radical **50**. The EPR spectrum
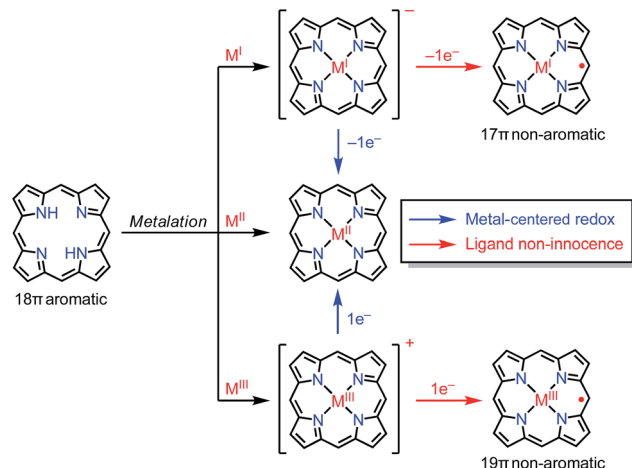

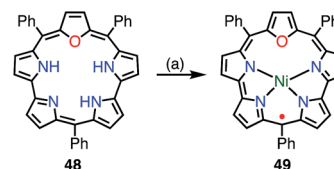**Fig. 14** General concept of ligand non-innocence in porphyrinoids.

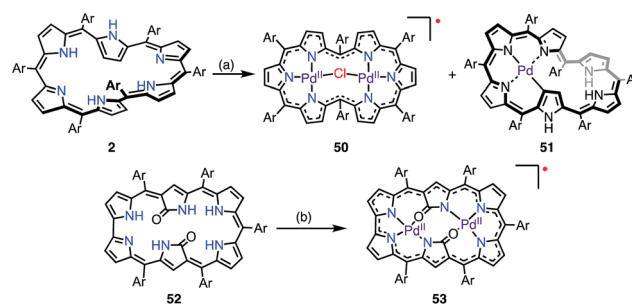**Fig. 15** Metalation with Ni(II) of oxasmaragdyrin. (a) 10 equiv. NiCl$_2$, DMF, reflux, 10 h, 10%.

Fig. 16 Metalation of hexaphyrins with Pd. (a) 10 equiv. PdCl$_2$, 10 equiv. NaOAc, CH$_2$Cl$_2$/MeOH, 45 °C, 24 h, 50% for **50**, 4% for **51**; (b) 10 equiv. Pd(OAc)$_2$, CH$_2$Cl$_2$/MeOH, rt, 10 h, 75%. Ar = pentafluorophenyl.

of **50** displayed a signal with an anisotropic *g*-factor of (2.0084, 1.9966, 1.9412), which indicated relatively strong spin–orbit coupling with the Pd(II) metal. The radical **50** is a rare example that has a delocalized spin over a non-planar conjugation circuit. Furuta *et al.* also reported a π-radical of a bis-Pd(II) complex of doubly N-confused hexaphyrin, *i.e.*, **52**, which had intriguing 2NH– and 3NH–NNNO cavities for metalation.[44] The bis-Pd complex **53** displayed an isotropic EPR signal at *g* = 2.0021. Despite the bulky *meso*-pentafluorophenyl groups, **53** adopted a π-stacked structure in the solid state with an interplanar distance of 3.266 Å, which was shorter than the sum of the van der Waals radii. This close arrangement may arise from a moderate intermolecular antiferromagnetic interaction owing to the overlap of the SOMOs, which was

proved by SQUID measurements (Weiss temperature of −42.9 K).

Sessler *et al.* recently reported the synthesis of the dicarbacorrole dimer **54**, in which the monomers share a fused vinylene moiety in the center (Fig. 17).[45] The macrocycle **54** has a symmetric structure with two trivalent CCNN cavities. The metalation of **54** with Cu afforded the mono- and bis-Cu(III) complexes **54Cu** and **54Cu₂**. Interestingly, the complex **54Cu** was further metalated with Pd(II) to give the neutral, stable π-radical **55** *via* spontaneous oxidation. The spin density of **55** was delocalized only over the Pd-dicarbacorrole segment, which was confirmed by EPR spectroscopy and theoretical calculations. This is a rare example in which the spin density is not fully delocalized over a flat conjugated system.

A valence mismatch between the ligand and metal is not necessary to induce ligand non-innocence. The [46]decaphyrin bis-Zn(II) complex **57** has a rigid structure and an inner cavity that is suitable for the coordination of a divalent metal in a linear manner. Osuka *et al.* examined the metalation of **57** with Cu(II) to obtain the unprecedented linearly coordinated Cu(II) complex **58'**.[46] However the resulting copper complex displayed a narrow EPR signal at $g = 2.0177$, which clearly indicated its purely organic π-radical character (Fig. 18). With the aid of theoretical calculations, the product was best interpreted as a Zn(II)−Cu(I)−Zn(II) complex of [45]decaphyrin, *i.e.*, **58**. These results indicated that almost instantaneous intramolecular electron transfer occurred from the decaphyrin ligand to the Cu(II) ion to generate the stable radical **58**. Interestingly, the 45π non-aromatic radical **58** exhibited a broad absorption band in the NIR region that extended to 2100 nm.

5.2. Tetraazaporphyrin phosphorus(v) complex

Kobayashi *et al.* reported the phosphorus(v) complex of tetraazaporphyrin **61** as an air-stable compound with a 19π electronic structure (Fig. 19).[15] The complex **61** was synthesized by the insertion of phosphorus(v) into **59** followed by reduction with triethylamine (TEA). Solid samples of **61** were inert under ambient conditions for a year. The exceptional stability of **61** was ascribed to the electron-deficient nature of tetraazaporphyrins, in which the four *meso*-carbons of porphyrin are replaced by four nitrogen atoms. It was also suggested that
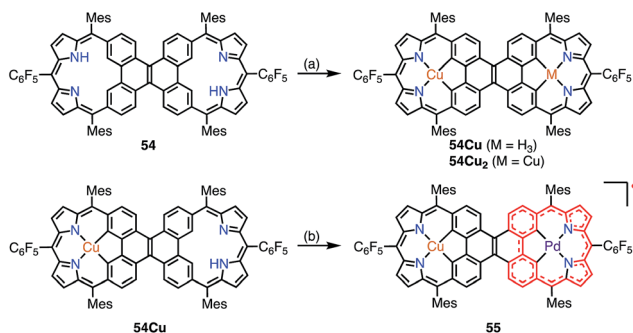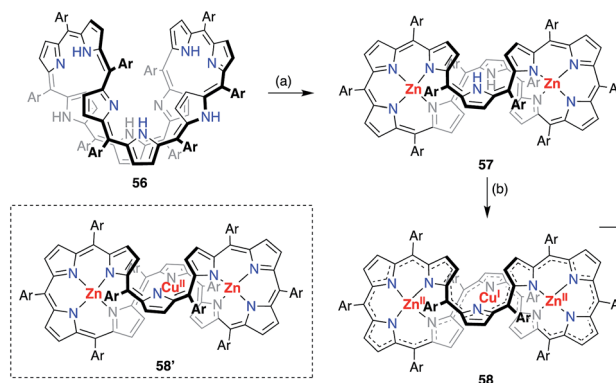

Fig. 18 Synthesis of the decaphyrin Zn(II)−Cu(I)−Zn(II) complex **58**. (a) 5 equiv. Zn(OAc)₂·2H₂O, 5 equiv. NaOAc, MeOH, reflux, 2 h, 61%; (b) 10 equiv. Cu(OAc)₂, 10 equiv. NaOAc, MeOH, rt, 4 h, 72%. Ar = pentafluorophenyl.
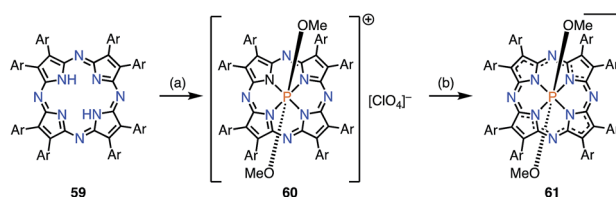

Fig. 19 Synthesis of **61**. (a) POBr₃ (200 equiv.), pyridine, 90 °C, 15 h, then CH₂Cl₂/MeOH, rt, 1 d. **60** was separated by SiO₂ column chromatography (CH₂Cl₂/MeOH/CF₃CO₂H = 90/9.5/0.5), then NaClO₄, CH₂Cl₂/MeCN, rt, 12 h, 56%; (b) **61** was separated by Al₂O₃ column chromatography (eluent: CH₂Cl₂/TEA = 99.5/0.5) without isolating **60**, 44%.

charge neutralization by the central cationic phosphorus atom and steric protection by the peripheral bulky groups were both important. The radical **61** exhibited a very low electrochemical oxidation potential of −0.36 V *vs.* Fc/Fc⁺ in *o*-dichlorobenzene.

5.3. Protonation-induced radical formation

Protonation of the pyrrolic nitrogen atoms in the inner cavity strongly affected both the electronic and the structural properties of expanded porphyrinoids.[47] For example, Naruta *et al.* synthesized the core-modified sapphyrin analogue **62**, which contained two exo-methylene bonds (Fig. 20). Protonation of **62** induced facile 2e⁻ oxidation to give the trication **63X₃** (X = Cl⁻, CF₃CO₂⁻).[48] The formation of **63X₃** was reversible, depending on the acid concentration, as evidenced by titration experiments. **63X₃** displayed a sharp EPR signal at $g = 2.0041$ and an NIR absorption band extending to 1400 nm, whereas the precursor **62** absorbed visible light up to 700 nm. X-ray diffraction analysis of **63X₃** revealed a distorted structure, which indicated minimal spin delocalization through the phenanthroline bridge. The intramolecular spin–spin interaction was proved by a SQUID study to be antiferromagnetic with $J/k_B = -680$ K. Besides these interesting redox behaviors upon protonation, **62** was also used as a fluorescent monitoring agent for sensing Mg²⁺ ions.[49]

Fig. 17 Metalation of dicarbacorroles with Cu(III) and Pd(II). (a) Cu(OAc)₂·H₂O in CHCl₃, reflux, 48 h; (b) Pd(PhCN)₂Cl₂ in PhCN, 180 °C, 2 h, 89%.

Fig. 20 Protonation behavior of the modified sapphyrin **62**.

was estimated to be short at 3.6 Å from the zero-field splitting value ($D = 57.7$ mT) on the assumption of the point dipole approximation. DFT calculations revealed the a_1'' and a_2'' symmetry of the SOMOs of the parent trication **68X$_3$** These MOs are non-disjoint and should be responsible for the ferromagnetic interaction.

5.4. "Hidden" non-innocence

A corrole **69** is a one-methine-carbon-contracted porphyrin that has three inner pyrrolic NH protons and thus acts as a trivalent ligand (Fig. 22).[52] In addition, corroles can incorporate metals in higher oxidation states such as Fe(v), Mn(vi), and Cr(vi). These complexes have often been used as mimics of biological intermediates.[53] Fe(iv), Ni(ii), and Cu(ii) corroles are all known as ligand-centered radical species.[54] Here, we review Cu(ii) corroles in detail.

Although the copper complex **70** was first synthesized in 1965,[55] its electronic structure and the oxidation state of the Cu center have for a long time been under discussion.[56] The observed diamagnetic character can be interpreted in terms of the Cu(iii) corrole **70A** or antiferromagnetically coupled Cu(ii) and the corrole radical cation **70B**. In 2010, Pierloot *et al.* suggested a non-innocent ligand character and a decreased singlet-triplet energy gap for **70** using *ab initio* calculations.[57] In 2005, Kadish *et al.* and Sarkar *et al.* independently reported the existence of non-innocent ligand character in Cu(ii) corroles by comparison with the corresponding silver corroles.[58a,b] The latter group also mentioned the existence of a mixed-orbital configuration in which the Cu corrole exists as an intermediate species between Cu(ii) and Cu(iii) complexes. In 2006, Lemon *et al.* further investigated the electronic structure of the copper corrole **70**.[58c] An EPR study of **70** showed a doublet signal with hyperfine coupling with a ^{65}Cu/^{63}Cu nucleus ($I = 3/2$), which is characteristic of Cu(ii) species. Further experimental support was given by X-ray photoelectron spectroscopy (XPS), which revealed shake-up satellite peaks in the Cu 2p region that were characteristic of Cu(ii) ions. The magnetic interaction between the corrole π-radical and the Cu(ii) center was found
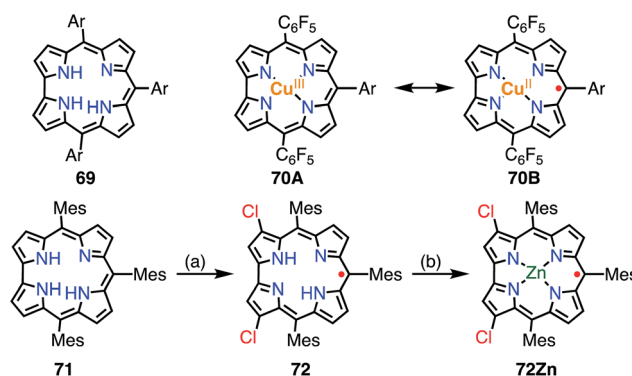

Fig. 21 Protonation-induced formation of the planar rosarin derivatives **64**. (a) Saturated Na$_2$S$_2$O$_4$ (aq), CH$_2$Cl$_2$, rt, 30 min, 87%; (b) MnO$_2$ or triethylamine; (c) HX (X = Cl, Br, I, CF$_3$CO$_3$, MeSO$_3$), CH$_2$Cl$_2$, rt; (d) HX (X = OTf, ClO$_4$), CH$_2$Cl$_2$, rt; (e) Me$_{10}$Fc, HI; (f) TBAX (X = Cl, Br, I), CH$_2$Cl$_2$, rt.

Sessler *et al.* reported the protonation behaviors of the *o*-phenylene-bridged annulated rosarin **64** (Fig. 21).[50] The protonation of **64** with HX (X = Cl, Br, CF$_3$CO$_2$, MeSO$_3$) afforded **66X$_2$** *via* a protonation-coupled electron transfer (PCET) process. The counterion has a great influence in this PCET process. For example, the protonation of **64** with HOTf or HClO$_4$ only gave the tri-protonation product **67X$_3$**, but the subsequent addition of tetrabutylammonium salts (*e.g.*, TBAX; X = Cl, Br) promoted the PCET process to give **66X$_2$**. When HI was used as an acid, the further reduction of **66X$_2$** to **65X** proceeded with decamethylferrocene.

Intriguingly, Fukuzumi *et al.* revealed that **67X$_3$** and the related rosarin derivatives **68X$_3$** were diradicals with 24π antiaromatic electronic structures.[51] The intramolecular spin–spin interaction was found by VT-EPR measurements to be only weakly ferromagnetic ($\Delta E_{ST} \approx +80$ J mol^{-1} at 4 K for **68X$_3$**). Despite the weak magnetic interaction, the spin–spin distance

Fig. 22 Two plausible electronic structures of Cu(ii) corrole (top) and corrole radicals. (a) WCl$_6$, W(CO)$_6$ (2 : 1), PhCN, 200 °C, 8 h, 4–7%; (b) Zn(OAc)$_2$·2H$_2$O, pyridine, 50 °C, 2 h, 77%. Ar = 4-methoxycarbonylphenyl.

by VT-NMR measurements to be strongly antiferromagnetic ($\Delta E_{ST} = -13.9 \pm 0.7$ kJ mol^{-1}). In this case, ligand-centered spin can only be observed when the paramagnetic character of the metal is eliminated, which is known as hidden non-innocence. The electronic structure of Cu corroles has been extensively discussed for decades from various experimental and theoretical aspects. However, further studies are required for a clear understanding of their electronic structure, in particular Cu(II)/Cu(III) mixed states and *meso*-substituent effects.

Recently, Bröring *et al.* synthesized the free corrole radical **72** and its Zn(II) complex **72Zn** by the oxidation of the *meso*-triarylcorrole **71**. Curiously, the oxidation of **71** with WCl$_6$ and W(CO)$_6$ gave compound **72** with concurrent β-chlorination, which indicated high spin densities on the β-carbons. Protection of these reactive β-positions is required for stabilization of the radicals.[59] Both **72** and **72Zn** were remarkably stable and exhibited split Soret-like bands around 400 nm and broad Q-like bands in the region of 500–800 nm.

Brückner *et al.* recently reported the Siamese-twin porphyrin **73**, which had a hexaphyrin-like skeleton with two pyrazole rings.[60] The free base **73** had a flexible structure without macrocyclic aromaticity. The bis-Cu(II) complex **74** was shown to be twisted and exhibit a ferromagnetic interaction with $J/k_B = +23.5$ K between the two $S = 1/2$ Cu(II) centers (Fig. 23). This magnetic interaction may arise from orbital orthogonality induced by the molecular twist. Two years later, Beer *et al.* investigated the oxidation of **74**.[61] Stepwise 1e$^-$ and 2e$^-$ oxidations of **74** were achieved with AgBF$_4$. The monocation **74(BF$_4$)** was found to be a species with a total $S = 1/2$, in which the two Cu(II) centers remained in the same oxidation state but the ligand was oxidized to the radical cation. The observed doublet spin indicated an antiferromagnetic interaction between the monoradical [**74**]$^+$ and the Cu(II) center. Moreover, the dication **74(BF$_4$)$_2$** was found to be a π-diradical, in which the two Cu(II) centers remained in the same oxidation state as determined by XAFS. X-ray diffraction analysis revealed the similar twisted structure of **74(BF$_4$)$_2$**, which was feasible for ferromagnetic coupling of the two Cu(II) centers. However, **74(BF$_4$)$_2$** exhibited

diamagnetic ($S = 0$) character. The authors suggested the ligand diradical character of [**74**]$^{2+}$, which coupled strongly with the Cu(II) center to cancel out the net spin. The π-diradical character of [**74**]$^{2+}$ may arise from the non-Kekulé nature of the dication owing to cross-conjugation between the pyrazole rings.

5.5. Magnetic interaction with the central metal

When a porphyrinoid π-radical has a paramagnetic metal in the central cavity, a magnetic interaction between the porphyrin radical ligand and the paramagnetic metal center is possible. Earlier, this was examined for the π-radical cation of *meso*-tetraphenyl Cu(II) porphyrin **75$^+$**, which was characterized as paramagnetic ($S = 1$ or $S = 1/2, 1/2$) in solution but diamagnetic ($S = 0$) in the solid state.[62,63] Orthogonality between the a$_u$ SOMO of the ligand and the d$_{x_2-y_2}$ orbitals of Cu(II) has been assigned as responsible for the ferromagnetic interaction. Therefore, the ferromagnetic interaction was observed in solution owing to the planar structure and the resulting strict orthogonality, but a slight structural distortion in the solid state gave rise to an antiferromagnetic interaction. It should be noted that other metalloporphyrin radical ions such as **76$^+$** and **77$^+$** have also been investigated as model compounds of compound I (Fig. 24).[64]

Square-planar Ni(II) porphyrins are usually diamagnetic (low-spin, $S = 0$), but become paramagnetic (high-spin, $S = 1$) upon the coordination of an additional ligand (Fig. 25).[65] The orbitals responsible for the spin of high-spin Ni(II) have σ-character, and the π-radicals should be orthogonal, which leads to a ferromagnetic interaction as in the case of Cu(II) porphyrins. Balch *et al.* reported that the β-octaethylporphyrin Ni(II) complex **21Ni** existed as a doublet species ($S = 1/2$) as a consequence of an antiferromagnetic interaction between the high-spin Ni(II) atom and the π-radical. On the other hand, Osuka *et al.* reported a strong ferromagnetic interaction in the *meso*-pentafluorophenylporphyrin Ni(II) complex **78Ni**.[66] The authors suggested that the balance of magnetic interactions between the central metal and the ligand radical was likely to be sensitive, so that a very small structural distortion could alter the magnetic interaction.
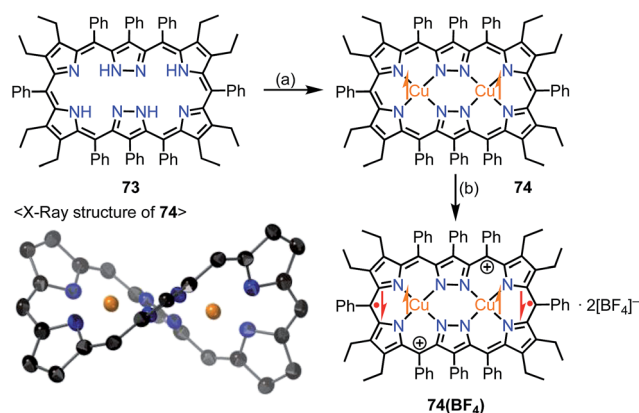
6. Kekulé/non-Kekulé radicals

Delocalized radicals can be divided into Kekulé and non-Kekulé molecules.[67] In most Kekulé-type diradicals, the loss of bond-formation energy due to the presence of two unpaired electrons is compensated by a gain in aromatic stabilization
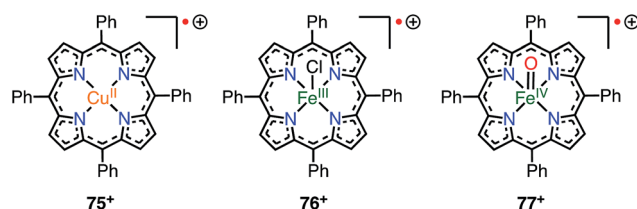

Fig. 23 Siamese–twin porphyrin and its Cu(II) complexes. (a) 4 equiv. Cu(OAc)$_2$·H$_2$O, CH$_2$Cl$_2$/MeOH, rt, overnight, 29%; (b) 2 equiv. AgBF$_4$ in EtNO$_2$, CH$_2$Cl$_2$, rt, 97%.

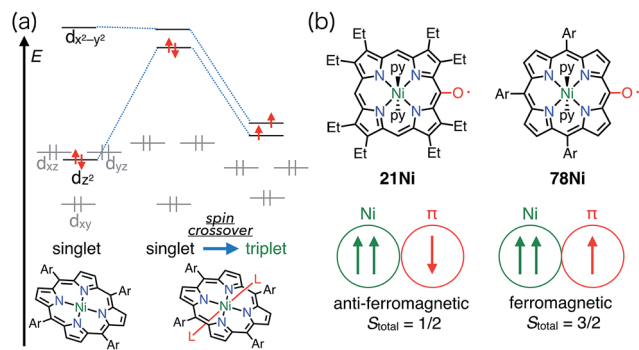**Fig. 24** Radical cations of metalloporphyrins.

Fig. 25 (a) Coordination-induced spin crossover of Ni(II) center. (b) OEP and 10,15,20-triarylporphyrin *meso*-oxy radicals and their magnetic interaction with the Ni(II) center. Ar = pentafluorophenyl.

Fig. 27 Thienylquinonoidal porphyrins and hexaphyrins. The *meso*-C_6F_5 groups in **84_1** and **84_2** are omitted for clarity.

energy.[68] On the other hand, non-Kekulé radicals have structures that cannot be drawn as a closed-shell form.

6.1. Quinonoidal porphyrinoids

5,10- and 5,15-quinonoidal porphyrins, which can be drawn as diradicals with the retention of the macrocyclic aromatic conjugation circuit, are also promising candidates for obtaining stable diradical species. However, the macrocyclic aromatic stabilization energy of porphyrin seems relatively small in comparison with the bond dissociation energy.[4] Consequently, the closed-shell quinonoidal electronic structure is more favorable, as seen in **34** and **79–82** (Fig. 26).[33,69–71] These quinonoidal porphyrinoids exhibit unique optical and electrochemical properties owing to decreased HOMO–LUMO gaps and perturbed aromaticity.

Osuka *et al.* prepared a series of 5,15-bis(3,5-di-*tert*-butyl-4-hydroxyphenyl-oligothienylene)-substituted porphyrins **83_n** and [26]hexaphyrins **84_n** (Fig. 27).[72] Whereas **83_0**, **84_0**, and **84_1** exhibited sharp ^1H NMR signals corresponding to a closed-shell quinonoidal structure, **83_1** and **84_2** remained silent or displayed broad signals even at low temperatures. Theoretical calculations at the UHF/6-31G*//B3LYP/6-31G* level revealed large diradical indices of 0.99 for **83_1** and 0.85 for **84_2**. Compound **83_1** was sufficiently stable for isolation but sensitive to air and moisture. This chemical instability implied

that the spin was less delocalized over the porphyrin core. On the other hand, **84_2** was highly stable, which was presumably due to effective spin delocalization over the hexaphyrin core, as indicated by DFT calculations. Judging from the exchange integral ($J/k_B = -33$ K for **83_1** and $J/k_B = -940$ K for **84_2**), the interaction between the two phenoxy radicals was slight in **83_1** in comparison with that in **84_2**, which also suggested that **83_1** was less conjugated. The strong antiferromagnetic interaction in **84_2** was presumably due to through-space spin–spin interactions, which are inaccessible for their porphyrin counterparts, as well as through-bond conjugation.

6.2. 2,18-Doubly linked corrole dimer

Shinokubo *et al.* synthesized the 2,18-doubly linked corrole dimer **85** with a cyclooctatetraene (COT) moiety in the center *via* oxidative fusion of a 2,2′-linked corrole dimer (Fig. 28).[73] **85** was quantitatively oxidized with DDQ to give **86**, and the metal complexes **85Co** and **86Zn** were also prepared. Whereas **85** and **85Co** displayed absorption spectra that were typical of aromatic corroles, **86** and **86Zn** exhibited largely perturbed spectra that extended to 1700 nm. **86Zn** was NMR-silent but EPR-active and displayed a sharp signal at $g = 2.0053$. **86** and **86Zn** were characterized as singlet diradicals. A SQUID study
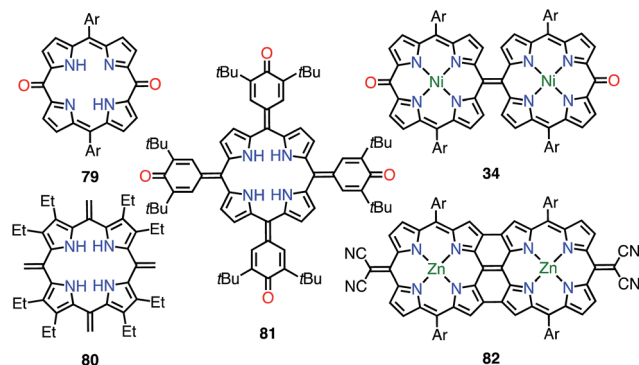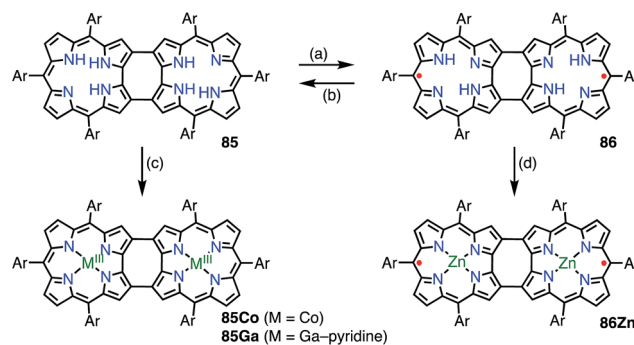

Fig. 26 Quinonoidal porphyrins.

Fig. 28 2,18-Doubly linked corrole dimers. (a) 5 equiv. DDQ, toluene, rt, 2 h, 83%; (b) NaBH$_4$, THF, rt, quant.; (c) 5 equiv. Co(OAc)$_2$, 7.8 equiv. PPh$_3$, EtOH, rt, 1.5 h, 78%; (d) sat. Zn(OAc)$_2$ in EtOH, CHCl$_3$, rt, 1 h, 54%. Ar = pentafluorophenyl.

of **86Zn** revealed an antiferromagnetic interaction with $J/k_B = -470$ K.

It is worth noting that the triply linked corrole dimer **87** also possessed a dimeric structure consisting of inner 2NH corroles, but **87** was a closed-shell molecule with a short C10–C10′ distance of 1.389 Å (Fig. 29).[74a] Recently, Gross et al. reported the synthesis and electronic structure of **85Ga**.[74b] The authors showed that the HOMO–1 of **85Ga**, which may correspond to the SOMO of the diradical **86**, had a very low spin density on C2 and C18, but a large coefficient on C15. The small extent of the overlap of the SOMOs may be the origin of the diradical character of **86** and **86Zn**.

6.3. Phenalenyl-fused porphyrins

Phenalenyl is a very important stable organic π-radical and has been extensively studied from both experimental and theoretical viewpoints.[75] Wu et al. prepared precursors of the mono- and bis-phenalenyl-fused porphyrins **88** and **90** via an intramolecular Friedel–Crafts reaction.[76] The authors concluded that the subsequent oxidation of **88** and **90** led to the formation of **89** and **91**, respectively (Fig. 30). Compound **89** was characterized as a closed-shell chromophore with a sharp ^{1}H NMR spectrum and a small diradical index of 0.06. Unfortunately, **91** was unstable under ambient conditions and gave the β-oxidized products **92** and **93**. The EPR signal of **91** displayed clear hyperfine coupling with two sets of protons, which was consistent with the proposed structure. DFT calculations suggested that **91** was a ground-state triplet diradical with $J/k_B \approx +1800$ K, although no experimental evidence in support of the
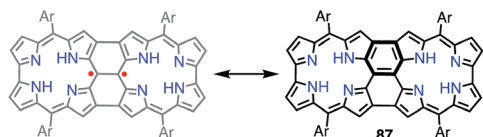
spin and oxidation state of **91** was reported. It is noteworthy that **91** formally bears two radicals on the sp[2]-carbon atoms attached to the meso-positions, but **91** cannot be drawn as a closed-shell structure owing to the externally fused conjugation circuit.

Osuka et al. also reported the similar peri-dinaphthoporphyrin **94**,[77] which comprises a partial structure of **91** and porphyrin tapes.[78] **94** was characterized as a closed-shell antiaromatic molecule (Fig. 31). Thompson et al. also prepared the bis-phenalenyl-fused porphyrin **95** by oxidative fusion followed by thermal dehydroaromatization.[79] However, **95** was a closed-shell molecule with a calculated diradical index of <3%. The clear difference between **91**, **94** and **95** is indicative that the design of the conjugation circuit is of great importance in producing a diradical.

6.4. Thermally induced radical character

Chmielewski et al. reported the synthesis of the pyrimidinenorcorrole dimer **99** via a unique ring expansion reaction of Ni(ɪɪ)-norcorrole **96** (Fig. 32).[80] **99** existed in equilibrium with its homolysis product **100** in toluene, which was proved by VT-EPR measurements and measurements of the temperature dependence of absorption. The population of **100** was estimated from VT-NMR measurements to be 12% at 300 K and almost 90% at 373 K. This process was reversible and reproducible in the open air, which indicated both the thermal stability and the chemical stability of **100**. Surprisingly, the dimerization of **100** was completely regioselective, whereas the spin density of **100** was fairly delocalized, as evidenced by both the hyperfine coupling constants observed in the EPR spectrum and DFT calculations. Moreover, **99** was further oxidized in DMF (even degassed and under N₂) to give **101**. The oxidation of **99** to **101** also proceeded in toluene with the aid of a catalyst. X-ray diffraction analysis revealed a molecular twist around the C3–C3′ bond with a dihedral angle of 44° and a relatively short C–C distance of 1.437 Å. In the solid state, a small amount of a paramagnetic species was observed (6% on the assumption of a triplet species) by a SQUID study. The EPR signal of **101** in the solid state displayed a fine structure with a zero-field splitting parameter of $D = 20$ mT, which is typical of triplet species. A VT-NMR study of the spin-lattice relaxation time (T_1) revealed that T_1 was shorter at 300 K (0.04–0.5 s) in comparison with its value

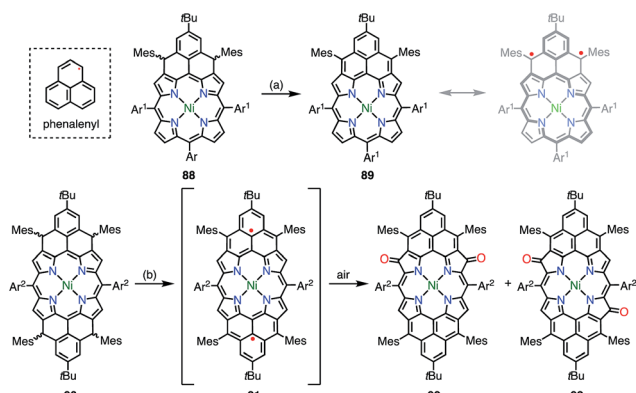**Fig. 29** Triply linked corrole dimer. Ar = pentafluorophenyl.

Fig. 30 Peripherally phenalenyl-fused porphyrins. Reagents and conditions: (a) 2 equiv. NIS, CH₂Cl₂, rt, 5 min, 49%; (b) 2 equiv. p-chloranil, CH₂Cl₂, rt, 10 min. **92** and **93** were obtained after exposure to air for 3.5 h, 20% for **92**, 39% for **93**. Ar¹ = 4-tert-butylphenyl, Ar² = 3,5-di-tert-butylphenyl.
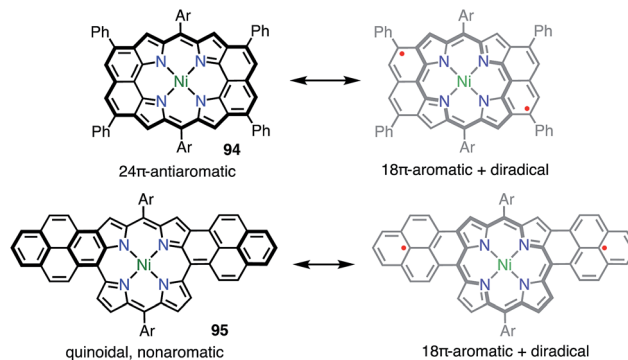

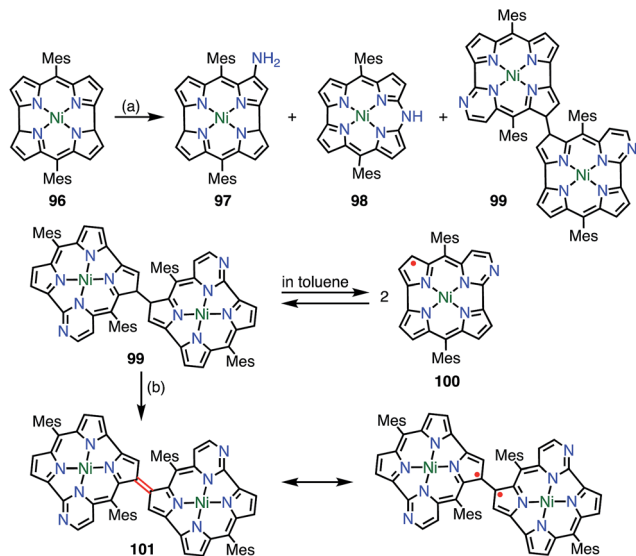**Fig. 31** Peripherally fused porphyrins. Ar = 3,5-di-tert-butylphenyl.

Fig. 32 Series of pyrimidinenorcorrole derivatives. (a) 12.5 equiv. 4-Amino-4H-1,2,4-triazole, 20 equiv. NaOH, THF, reflux, 2 h, 8.6% for **97**, 28.8% for **98**, 3.3% for **99**, 32.2% for **100**; (b) degassed DMF, N_2, 80 °C, 30 min, 98%.

at 183 K ($T_1 > 1$ s), which indicated thermally enhanced paramagnetic character. Rotation around the C3–C3′ bond was also observed in the form of averaging of the signals due to the *meso*-mesityl groups. The authors proposed that the population of the paramagnetic form was higher and/or chemical exchange between the forms was faster upon heating. These phenomena were further supported by quantum calculations that showed that the S–T gap was dependent on the dihedral angle.

Wu *et al.* also proposed the thermally induced diradical characters of the 5,15-bis(9-fluorenylidene)porphyrin **102** and its Ni complex **102Ni** (Fig. 33).[81] Both **102** and **102Ni** adopted quinonoidal structures in the single-crystal state with distortions due to steric hindrance by the fluorenyl groups. X-ray analysis revealed the highly bent structure of **102** due to steric
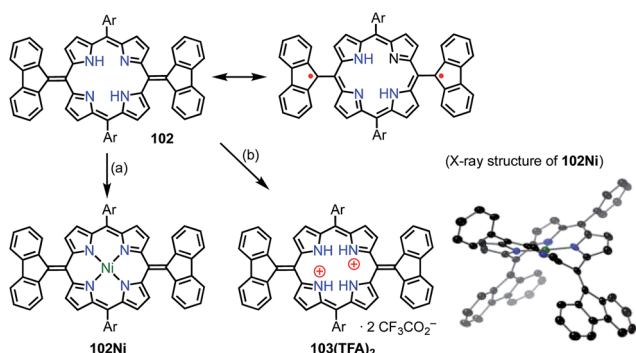
repulsion between the β-proton and the fluorenyl group with a short C_{meso}–$C_{fluorenyl}$ bond length of 1.35–1.37 Å. A VT-NMR study detected signal broadening at high temperatures, which indicated the structural flexibility of **102** and **102Ni**. **102Ni** exhibited signal broadening at lower temperatures than **102**, which has been interpreted in terms of the conformational flexibility of **102Ni**, despite its metalation. A SQUID study of **102** and **102Ni** revealed unusual open hysteresis loops for net magnetization.[82] The estimated value of ΔE_{ST} was higher in **102** than in **102Ni**, which was consistent with the VT-NMR results. From these results and DFT calculations, the authors proposed that the diradical character was triggered by a thermally induced "butterfly-like" structural change. Protonation also altered the diradical character of **102**. For example, protonation of **102** gave **103(TFA)₂** in quantitative yield, which exhibited sharp NMR signals even at high temperatures, which indicated closed-shell character.

In the case of **102**, structural flexibility induced the diradical character. Very recently, Osuka *et al.* reported a contrasting system in which diradical character was enhanced *via* structural rigidification.[83] As shown above, the 5,5′-linked 15,15′-dioxo-Ni(ɪɪ)-diporphyrin **34** was known to be a closed-shell quinonoid with a distorted structure. It was considered that the replacement of the central metal would lead to changes in the structure and thus magnetic interactions. In fact, the Ni(ɪɪ) complex **104Ni** was a closed-shell quinonoid similar to **34**, but the Zn(ɪɪ) complex **105ZnIm** was found to be a stable diradical (Fig. 34). X-ray diffraction analysis of **105ZnIm** showed a perpendicular structure consisting of two highly planar porphyrin segments with a dihedral angle of 71°. The C5–C5′ bond length (1.492 Å) clearly indicated single-bond character. These structural features indicated a diradical electronic state, which was supported by the silent ¹H NMR spectrum, the active EPR spectrum, magnetism detected by SQUID experiments, a broad absorption tail extending to 1800 nm, and DFT calculations. Moreover, the free base **104H₂** was found to exist as an equilibrium mixture of the closed-shell quinonoid **104H₂** and the diradical **105H₂** (**104H₂**/**105H₂** = 81/19 in toluene at room temperature), as evidenced by VT-EPR and VT-NMR studies. The contribution of **105H₂** increased at high temperatures.

Fig. 33 5,15-Bis(9-fluorenyl)porphyrins and X-ray crystal structure of **102Ni**. (a) 10 equiv. Ni(OAc)₂·4H₂O, toluene, 120 °C, 5 h, quant.; (b) 2 equiv. CF₃CO₂H, CH₂Cl₂, <10 min, quant. Ar = 3,5-di-*tert*-butylphenyl. Hydrogen atoms and *tert*-butyl groups in the crystal structure of **102Ni** are omitted for clarity.
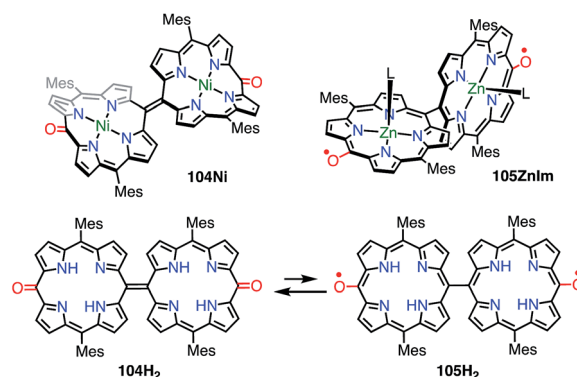

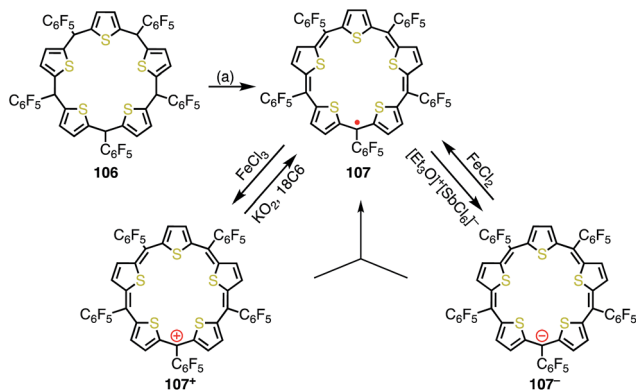**Fig. 34** 5,5′-Linked 15,15′-dioxodiporphyrins. L = N-methylimidazole.

Fig. 35 Synthesis and redox behavior of pentathiapentaphyrin **107**. (a) FeCl$_3$, CH$_2$Cl$_2$, rt, 1 h, then triethylamine, rt, 38%.

7. Other example

7.1. Pentathiapentaphyrin

Anand *et al.* reported the synthesis of pentathiapentaphyrin(1.1.1.1.1) **107**,[84] which cannot be drawn as a neutral closed-shell form without an unpaired electron, in a similar way to the corrole radical **72** (Fig. 35). X-ray crystallographic analysis revealed its planar structure, which was suitable for spin delocalization. In fact, **107** displayed high stability towards air and moisture. The radical **107** could be reversibly oxidized/reduced to give the 24π anti-aromatic cation **107$^+$** and the 26π aromatic anion **107$^-$**, respectively. The mixing of **107$^+$** and **107$^-$** formed **107**, which indicated the high tendency to comproportionation and thus the high stability of **107**.

8. Conclusion and perspectives

We reviewed porphyrinoid-based stable radicals mainly from the viewpoints of radical structure and stability. Early research focused on porphyrinoid-based radicals as important reaction intermediates in biochemistry. Recently, interest has been shifting to the investigation of functional materials based on stable radicals. The remarkable stability of porphyrinoid radicals is mainly due to effective spin delocalization (thermal stabilization). However, in some cases steric protection at positions where relatively high spin density is localized (kinetic stabilization) is necessary for chemical stability. The effective spin delocalization ability of porphyrinoids can be attributed to their unique structural and electronic flexibilities. Reflecting their delocalized π-radical characters, these radicals generally exhibit unique properties such as NIR absorption bands, magnetic properties, and small redox gaps.

There is ample room for further functionalization of stable porphyrinoids by taking advantage of their stability as well as properties such as light-harvesting functions, structural flexibility, and metal-coordinating ability. Owing to their chemical stability and unique properties, porphyrinoid-based radicals are promising candidates for future applications. The precise alignment of radicals in the solid and liquid-crystalline phases is required to achieve effective bulk properties, but general guidelines for the design of packing structures have not yet been established. Most of the stable radicals that have been synthesized so far are [4n + 1]π-species, and the stabilization of [4n + 3]π electronic radicals (and radical anions) still remains a challenging topic. The investigation of general strategies for stabilizing such electron-rich π-radicals will be important, because it will help in the creation of novel functional molecules. A recent study revealed the triplet Baird-type aromaticity of an internally dithienothiophene-bridged [34]octaphyrin dication.[85] The excited-state dynamics of porphyrinoid-based radicals are also of great interest.

In addition, porphyrinoids may be promising for stabilizing radical-related unstable chemical species such as carbenes, nitrenes and other reactive species.[86,87] Related studies are actively in progress in our laboratory, and we hope to report their results in the near future.

Conflicts of interest

There are no conflicts to declare.

Acknowledgements

Notes and references

1 (*a*) *Handbook of Porphyrin Science*, ed. K. M. Kadish, K. M. Smith and R. Guilard, World Scientific Publishing, Singapore, 2010, vol. 1–25; (*b*) *The Porphyrin Handbook*, ed. K. M. Kadish, K. M. Smith and R. Guilard, Academic Press, San Diego, 2000, vol. 1–10; (*c*) A. Osuka, E. Tsurumaki and T. Tanaka, *Bull. Chem. Soc. Jpn.*, 2011, **84**, 679; (*d*) C. G. Claessens, D. González-Rodríguez, M. S. Rodríguez-Morgade, A. Medina and T. Torres, *Chem. Rev.*, 2014, **114**, 2192; (*e*) S. Shimizu, *Chem. Rev.*, 2017, **117**, 2730; (*f*) S. Saito and A. Osuka, *Angew. Chem., Int. Ed.*, 2011, **50**, 4342; (*g*) A. Osuka and S. Saito, *Chem. Commun.*, 2011, **47**, 4330; (*h*) T. Tanaka and A. Osuka, *Chem. Rev.*, 2017, **117**, 2584; (*i*) B. Szyszko, M. J. Białek, E. Pacholska-Dudziak and L. Latos-Grażyński, *Chem. Rev.*, 2017, **117**, 2839.

2 (*a*) J. P. McEvoy and G. W. Brudvig, *Chem. Rev.*, 2006, **106**, 4455; (*b*) P. Hlavica, *Eur. J. Biochem.*, 2004, **271**, 4335.

3 (*a*) Y. Yamamoto, Y. Hirata, M. Kodama, T. Yamaguchi, S. Matsukawa, K. Akiba, D. Hashizume, F. Iwasaki, A. Muranaka, M. Uchiyama, P. Chen, K. M. Kadish and N. Kobayashi, *J. Am. Chem. Soc.*, 2010, **132**, 12627; (*b*) S. Sugawara, Y. Hirata, S. Kojima, Y. Yamamoto, E. Miyazaki, K. Takimiya, S. Matsukawa, D. Hashizume, J. Mack, N. Kobayashi, Z. Fu, K. M. Kadish, Y. M. Sung, K. S. Kim and D. Kim, *Chem.–Eur. J.*, 2012, **18**, 3566; (*c*) M. Pohl, H. Schmisckler, J. Lex and E. Vogel, *Angew. Chem., Int. Ed. Engl.*, 1991, **31**, 1693; (*d*) C. Liu, D.-M. Shen and Q.-Y. Chen, *J. Am. Chem. Soc.*, 2007, **129**, 5814.

4 (a) J. Aihara, *J. Phys. Chem. A*, 2008, **112**, 5305; (b) J. L. Wu, I. Fernandez and P. v. R. Schleyer, *J. Am. Chem. Soc.*, 2013, **135**, 315; (c) J. Aihara and H. Horibe, *Org. Biomol. Chem.*, 2009, **7**, 1939; (d) M. Makino and J. Aihara, *J. Phys. Chem. A*, 2012, **116**, 8074.

5 (a) T. Asakura, J. S. Leigh Jr., H. R. Drott, T. Yonetani and B. Chance, *Proc. Natl. Acad. Sci. U. S. A.*, 1971, **68**, 861; (b) M. H. Rakowski, K. M. More, A. V. Kulikov, G. R. Eaton and S. S. Eaton, *J. Am. Chem. Soc.*, 1995, **117**, 2049.

6 T. T. H. Tram, Y.-R. Chang, T. K. A. Hoang, M.-Y. Kuo and Y. O. Su, *J. Phys. Chem. A*, 2016, **120**, 5511.

7 J. Rittle and M. T. Green, *Science*, 2010, **330**, 933.

8 (a) T. Satoh, M. Minoura, H. Nakano, K. Furukawa and Y. Matano, *Angew. Chem., Int. Ed.*, 2016, **55**, 2235; (b) K. Sudoh, T. Satoh, T. Amaya, K. Furukawa, M. Minoura, H. Nakano and Y. Matano, *Chem.–Eur. J.*, 2017, **23**, 16364.

9 A. Yamaji, H. Tsurugi, Y. Miyake, K. Mashima and H. Shinokubo, *Chem.–Eur. J.*, 2016, **22**, 3956.

10 N. Fukui, W. Cha, D. Shimizu, J. Oh, K. Furukawa, H. Yorimitsu, D. Kim and A. Osuka, *Chem. Sci.*, 2017, **8**, 189.

11 N. Fukui, H. Yorimitsu and A. Osuka, *Chem.–Eur. J.*, 2016, **22**, 18476.

12 J. Mack and M. J. Stillman, *J. Porphyrins Phthalocyanines*, 2001, **5**, 67.

13 T. Koide, G. Kashiwazaki, M. Suzuki, K. Furukawa, M.-C. Yoon, S. Cho, D. Kim and A. Osuka, *Angew. Chem., Int. Ed.*, 2008, **47**, 9661.

14 H. Rath, S. Tokuji, N. Aratani, K. Furukawa, J. M. Lim, D. Kim, H. Shinokubo and A. Osuka, *Angew. Chem., Int. Ed.*, 2010, **49**, 1489.

15 T. Yoshida, W. Zhou, T. Furuyama, D. B. Leznoff and N. Kobayashi, *J. Am. Chem. Soc.*, 2015, **137**, 9258.

16 J. Rawson, P. J. Angiolillo and M. J. Therien, *Proc. Natl. Acad. Sci. U. S. A.*, 2015, **112**, 13779.

17 M. D. Peeks, C. E. Tait, P. Neuhaus, G. M. Fischer, M. Hoffmann, R. Haver, A. Cnossen, J. R. Hammer, C. R. Timmel and H. L. Anderson, *J. Am. Chem. Soc.*, 2017, **139**, 10461.

18 (a) T. Yoshida, M. Noguchi, G. Kikuchi and S. Sano, *J. Biochem.*, 1981, **90**, 125; (b) S. Sano, T. Sano, I. Morishima, Y. Shiro and Y. Maeda, *Proc. Natl. Acad. Sci. U. S. A.*, 1986, **83**, 531; (c) A. Wilks and P. R. O. de Montellano, *J. Biol. Chem.*, 1993, **268**, 22357; (d) A. Gossauer, *Chimia*, 1994, **48**, 352.

19 K. M. Matera, S. Takahashi, H. Fujii, H. Zhou, K. Ishikawa, T. Yoshimura, D. L. Rousseau, T. Yoshida and M. Ikeda-Saito, *J. Biol. Chem.*, 1996, **271**, 6618.

20 R. Bonnett, M. J. Dimsdale and K. D. Sales, *Chem. Commun.*, 1970, 962.

21 A. L. Balch, B. C. Noll and E. P. Zovinka, *J. Am. Chem. Soc.*, 1992, **114**, 3380.

22 J.-H. Fuhrhop, S. Besecke, J. Subramanian, C. Mengersen and D. Riesner, *J. Am. Chem. Soc.*, 1975, **97**, 7141.

23 A. L. Balch, *Coord. Chem. Rev.*, 2000, **200–202**, 349.

24 A. L. Balch, B. C. Noll, S. L. Phillips, S. M. Reid and E. P. Zovinka, *Inorg. Chem.*, 1993, **32**, 4730.

25 R. G. Khoury, L. Jaquinod, A. M. Shachter, N. Y. Nelson and K. M. Smith, *Chem. Commun.*, 1997, 215.

26 R. G. Khoury, L. Jaquinod, R. Paolesse and K. M. Smith, *Tetrahedron*, 1999, **55**, 6713.

27 T. Koide, K. Furukawa, H. Shinokubo, J.-Y. Shin, K. S. Kim, D. Kim and A. Osuka, *J. Am. Chem. Soc.*, 2010, **132**, 7246.

28 M. Ishida, J.-Y. Shin, J. M. Lim, B. S. Lee, M.-C. Yoon, T. Koide, J. L. Sessler, A. Osuka and D. Kim, *J. Am. Chem. Soc.*, 2011, **133**, 15533.

29 D. Shimizu, J. Oh, K. Furukawa, D. Kim and A. Osuka, *Angew. Chem., Int. Ed.*, 2015, **54**, 6613.

30 D. Shimizu, J. Oh, K. Furukawa, D. Kim and A. Osuka, *J. Am. Chem. Soc.*, 2015, **137**, 15584.

31 L. J. Esdaile, M. O. Senge and D. P. Arnold, Partial formation of similar meso-oxy radical had been suggested before, but isolation or characterization had not been achieved, *Chem. Commun.*, 2006, 4192.

32 (a) H. Song, R. D. Orosz, C. A. Reed and R. Scheidt, *Inorg. Chem.*, 1990, **29**, 4274; (b) W. R. Scheidt, K. E. Brancato-Buentello, H. Song, K. V. Reddy and B. Cheng, *Inorg. Chem.*, 1996, **35**, 7500; (c) K. M. Barkigia, M. W. Renner and J. Fajer, *J. Phys. Chem. B*, 1997, **101**, 8398.

33 L. J. Esdaile, L. Rintoul, M. S. Goh, K. Merahi, N. Parizel, R. M. Wellard, S. Choua and D. P. Arnold, *Chem.–Eur. J.*, 2016, **22**, 3403.

34 K. Fujimoto, J. Oh, H. Yorimitsu, D. Kim and A. Osuka, *Angew. Chem., Int. Ed.*, 2016, **55**, 3196.

35 N. Fukui, W.-Y. Cha, S. Lee, S. Tokuji, D. Kim, H. Yorimitsu and A. Osuka, *Angew. Chem., Int. Ed.*, 2013, **52**, 9728.

36 K. Kato, W. Cha, J. Oh, K. Furukawa, H. Yorimitsu, D. Kim and A. Osuka, *Angew. Chem., Int. Ed.*, 2016, **55**, 8711.

37 A. Wakamiya and S. Yamaguchi, *Bull. Chem. Soc. Jpn.*, 2015, **88**, 1357.

38 K. Kato, K. Furukawa, T. Mori and A. Osuka, *Chem.–Eur. J.*, 2018, **24**, 572.

39 R. G. Hicks, *Org. Biomol. Chem.*, 2007, **5**, 1321.

40 D. Shimizu, S. K. Lee, D. Kim and A. Osuka, *Chem.–Asian J.*, 2016, **11**, 2946.

41 D. Shimizu, K. Furukawa and A. Osuka, *Angew. Chem., Int. Ed.*, 2017, **56**, 7435.

42 (a) P. J. Chirik, *Inorg. Chem.*, 2011, **50**, 9737; (b) V. Lyaskovskyy and B. de Bruin, *ACS Catal.*, 2012, **2**, 270.

43 B. Sridevi, S. Jeyaprakash, R. Rao, T. K. Chandrashekar, U. Englich and K. Ruhlandt-Senge, *Inorg. Chem.*, 2000, **39**, 3669.

44 Y. Hisamune, K. Nishimura, K. Isakari, M. Ishida, S. Mori, S. Karasawa, T. Kato, S. Lee, D. Kim and H. Furuta, *Angew. Chem., Int. Ed.*, 2015, **54**, 7323.

45 X.-S. Ke, Y. Hong, P. Tu, Q. He, V. M. Lynch, D. Kim and J. L. Sessler, *J. Am. Chem. Soc.*, 2007, **139**, 15232.

46 Y. Tanaka, T. Yoneda, K. Furukawa, T. Koide, H. Mori, T. Tanaka, H. Shinokubo and A. Osuka, *Angew. Chem., Int. Ed.*, 2015, **54**, 10908.

47 S. Zakavi, R. Omidyan and S. Talebzadeh, *RSC Adv.*, 2016, **6**, 82219.

48 M. Ishida, S. Karasawa, H. Uno, F. Tani and Y. Naruta, *Angew. Chem., Int. Ed.*, 2010, **49**, 5906.

49 M. Ishida, Y. Naruta and F. Tani, *Angew. Chem., Int. Ed.*, 2010, **49**, 91.

50 M. Ishida, S.-J. Kim, C. Preihs, K. Ohkubo, J. M. Lim, B. S. Lee, J. S. Park, V. M. Lynch, V. V. Roznyatovskiy, T. Sarma, P. K. Panda, C.-H. Lee, S. Fukuzumi, D. Kim and J. L. Sessler, *Nat. Chem.*, 2013, **5**, 15.

51 S. Fukuzumi, K. Ohkubo, M. Ishida, C. Preihs, B. Chen, W. T. Borden, D. Kim and J. L. Sessler, *J. Am. Chem. Soc.*, 2015, **137**, 9780.

52 K. E. Thomas, A. B. Alemayehu, J. Conradie, C. M. Beavers and A. Ghosh, *Acc. Chem. Res.*, 2012, **45**, 1203.

53 S. Shaik, S. Cohen, Y. Wang, H. Chen, D. Kumar and W. Thiel, *Chem. Rev.*, 2010, **110**, 949.

54 (a) E. Vogel, S. Will, A. S. Tilling, L. Neumann, J. Lex, E. Bill, A. X. Trautwein and K. Wieghardt, *Angew. Chem., Int. Ed. Engl.*, 1994, **33**, 731; (b) S. Will, J. Lex, E. Vogel, H. Schmickler, J.-P. Gisselbrecht, C. Haubtmann, M. Bernard and M. Gross, *Angew. Chem., Int. Ed. Engl.*, 1997, **36**, 357.

55 A. W. Johnson and I. T. Kay, *J. Chem. Soc.*, 1965, 1620.

56 (a) A. W. Johnson, *Pure Appl. Chem.*, 1971, **28**, 195; (b) N. S. Hush and J. M. Dyke, *J. Inorg. Nucl. Chem.*, 1973, **35**, 4341; (c) N. S. Hush and J. M. Dyke, *J. Chem. Soc., Dalton Trans.*, 1974, 395; (d) M. Bröring, F. Brégier, E. C. Tejero, C. Hell and M. C. Holthausen, *Angew. Chem., Int. Ed.*, 2007, **46**, 445.

57 K. Pierloot, H. Zhao and S. Vancoillie, *Inorg. Chem.*, 2010, **49**, 10316.

58 (a) K. E. Thomas, H. Vazquez-Lima, Y. Fang, Y. Song, K. J. Gagnon, C. M. Beavers, K. M. Kadish and A. Ghosh, *Chem.–Eur. J.*, 2015, **21**, 16839; (b) W. Sinha, M. G. Sommer, N. Deibel, F. Ehret, M. Bauer, B. Sarkar and S. Kar, *Angew. Chem., Int. Ed.*, 2015, **54**, 13769; (c) C. M. Lemon, M. Huynh, A. G. Maher, B. L. Anderson, E. D. Bloch, D. C. Powers and D. G. Nocera, *Angew. Chem., Int. Ed.*, 2016, **55**, 2176.

59 P. Schweyen, K. Brandhorst, R. Wicht, B. Wolfram and M. Bröring, *Angew. Chem., Int. Ed.*, 2015, **54**, 8213.

60 L. K. Frensch, K. Pröpper, M. John, S. Demeshko, C. Brückner and F. Meyer, *Angew. Chem., Int. Ed.*, 2011, **50**, 1420.

61 L. K. Blusch, K. E. Craigo, V. Martin-Diaconescu, A. B. McQuarters, E. Bill, S. Dechert, S. DeBeer, N. Lehnert and F. Meyer, *J. Am. Chem. Soc.*, 2013, **135**, 13892.

62 (a) J. H. Fuhrhop and D. Mauzerall, *J. Am. Chem. Soc.*, 1969, **91**, 4174; (b) A. Wolberg and J. Manassen, *J. Am. Chem. Soc.*, 1970, **92**, 2982; (c) C. Mangersen, J. Subramanian and J.-H. Fuhrhop, *Mol. Phys.*, 1976, **32**, 893; (d) D. Dolphin, Z. Muljiani, K. Rousseau, D. C. Borg, J. Fajer and R. H. Felton, *Ann. N. Y. Acad. Sci.*, 1973, **206**, 177.

63 W. F. Scholz, C. A. Reed, Y. J. Lee, W. R. Scheidt and G. Lang, *J. Am. Chem. Soc.*, 1982, **104**, 6791.

64 (a) A. Wolberg and J. Manassen, *J. Am. Chem. Soc.*, 1970, **92**, 2982; (b) J. T. Groves, R. C. Haushalter, M. Nakamura, T. E. Nemo and B. J. Evans, *J. Am. Chem. Soc.*, 1981, **103**,

2884; (c) P. Gans, G. Buisson, E. Duée, J.-C. Marchon, B. S. Erler, W. F. Scholz and C. A. Reed, *J. Am. Chem. Soc.*, 1986, **108**, 1223.

65 S. Thies, H. Sell, C. Bornholdt, C. Schütt, F. Köhler, F. Tuczek and R. Herges, *Chem.–Eur. J.*, 2012, **18**, 16358.

66 C. Stähler, D. Shimizu, K. Yoshida, K. Furukawa, R. Herges and A. Osuka, *Chem.–Eur. J.*, 2017, **23**, 7217.

67 M. Abe, *Chem. Rev.*, 2013, **113**, 7011.

68 Z. Zeng, X. Shi, C. Chi, J. T. L. Navarrete, J. Casado and J. Wu, *Chem. Soc. Rev.*, 2015, **44**, 6578.

69 C. Otto and E. Breitmaier, *Liebigs Ann.*, 1991, 1347.

70 J. P. Hill, I. J. Hewitt, C. E. Anson, A. K. Powell, A. L. McCarty, P. A. Karr, M. E. Zandler and F. D'Souza, *J. Org. Chem.*, 2004, **69**, 5861.

71 I. M. Blake, A. K. Krivokapic, M. Katterle and H. L. Anderson, *Chem. Commun.*, 2002, 1662.

72 K. Naoda, D. Shimizu, J. O. Kim, K. Furukawa, D. Kim and A. Osuka, *Chem.–Eur. J.*, 2017, **23**, 8969.

73 S. Hiroto, K. Furukawa, H. Shinokubo and A. Osuka, *J. Am. Chem. Soc.*, 2006, **128**, 12380.

74 (a) S. Ooi, T. Tanaka, K.-H. Park, D. Kim and A. Osuka, *Angew. Chem., Int. Ed.*, 2016, **55**, 6535; (b) S. Bhowmik, M. Kosa, A. Mizrahi, N. Fridman, M. Saphier, A. Stanger and Z. Gross, *Inorg. Chem.*, 2017, **56**, 2287.

75 T. Kubo, *Chem. Rec.*, 2015, **15**, 218.

76 W. Zeng, S. Lee, M. Son, M. Ishida, K. Furukawa, P. Hu, Z. Sun, D. Kim and J. Wu, *Chem. Sci.*, 2015, **6**, 2427.

77 M. Umetani, K. Naoda, T. Tanaka, S.-K. Lee, J. Oh, D. Kim and A. Osuka, *Angew. Chem., Int. Ed.*, 2016, **55**, 6305.

78 A. Tsuda and A. Osuka, *Science*, 2001, **293**, 5527.

79 V. V. Diev, D. Femia, Q. Zhong, P. I. Djurovich, R. Haiges and M. E. Thompson, *Chem. Commun.*, 2016, **52**, 1949.

80 B. Kin, T. Yoshida, X. Li, M. Stępień, H. Shinokubo and P. J. Chmielewski, *Angew. Chem., Int. Ed.*, 2016, **55**, 13142.

81 H. Zhang, H. Plan, T. S. Herng, T. Y. Gopalakrishna, W. Zeng, J. Ding and J. Wu, *Angew. Chem., Int. Ed.*, 2017, **56**, 13484.

82 Similar hysteresis behaviors were also observed for structurally flexible diradicals, but they showed closed hysteresis loop or phase transition behavior: (a) T. Li, G. Tan, D. Shao, J. Li, Z. Zhang, Y. Song, Y. Sui, S. Chen, Y. Fang and X. Wang, *J. Am. Chem. Soc.*, 2016, **138**, 10092; (b) Y. Su, X. Wang, L. Wang, Z. Zhang, X. Wang, Y. Song and P. P. Power, *Chem. Sci.*, 2016, **7**, 6514.

83 Y. Jun-i, N. Fukui, K. Furukawa and A. Osuka, DOI: 10.1002/chem.201705769.

84 T. Y. Gopalakrishna, J. S. Reddy and V. G. Anand, *Angew. Chem., Int. Ed.*, 2014, **53**, 10984.

85 W.-Y. Cha, T. Kim, A. Ghosh, Z. Zhang, X.-S. Ke, R. Ali, V. M. Lynch, J. Jung, W. Kim, S. Lee, S. Fukuzumi, J. S. Park, J. L. Sessler, T. K. Chandrashekar and D. Kim, *Nat. Chem.*, 2017, **9**, 1243.

86 E. Iwamoto, K. Hirai and H. Tomioka, *J. Am. Chem. Soc.*, 2003, **125**, 14664.

87 F. Dielmann, O. Back, M. Henry-Ellinger, P. Jerabek, G. Frenking and G. Bertrand, *Science*, 2012, **337**, 1526.